



Unsteady free-surface flow induced by a line sink

T.E. STOKES¹, G.C. HOCKING² and L.K. FORBES³

¹*Department of Mathematics, University of Waikato, Private Bag 3105, Hamilton, New Zealand*
(e-mail: stokes@math.waikato.ac.nz)

²*Mathematics and Statistics, Murdoch University, Murdoch, WA, 6150, Australia*
(e-mail: G.Hocking@murdoch.edu.au)

³*School of Mathematics and Physics, University of Tasmania, GPO Box 252-37, Hobart, TAS, 7001, Australia*
(e-mail: Larry.Forbes@utas.edu.au)

Received 2 August 2001; accepted in revised form 20 May 2003

Abstract. The unsteady flow of fluid from a deep reservoir through a line sink beneath a free surface with surface tension is considered. Two different initial conditions are discussed; the first effectively represents impulsive withdrawal from rest, and the second can be regarded as a disturbance to an existing steady flow. Small-time expansions and numerical methods are used to investigate both the movement to steady states and the critical drawdown of the free surface in the two situations. It is shown that there are several different critical values of flow parameters at which the flow changes its nature. In the zero-surface-tension case, the situation is not fully resolved, but the addition of surface tension clarifies the flow behaviour greatly, and drawdown or movement to a steady state becomes evident. For the second class of initial conditions, it appears that either movement to a steady state or drawdown are the only subcritical possibilities.

Key words: fluid withdrawal, free-surface flow, line sink, surface tension

1. Introduction

Flow generated during water withdrawal is of undoubted importance, both to reservoir management and to maintenance of water quality (see *e.g.* [1]). Withdrawal from layers of water can change the stratification significantly and generate internal wave activity. It can even allow short-circuiting of inflows (on time scales of the order of the residence time) by the withdrawal of fluid from a horizontal river-flow intrusion almost as it arrives.

Withdrawal from fluids with a linear stratification was the first of such flows to be understood in any detail. Early work gave a withdrawal layer of a thickness dependent on the degree of stratification and the flow rate, see *e.g.* [2]. Problems with general stratification are more difficult to solve, but provided there are no sharp discontinuities, general behaviour can be surmised reasonably well by averaging of the gradient.

In contrast, the problem in which there are two or more layers of uniform but different density separated by a thin interface has proven very difficult. It is known that in this situation all of the withdrawn water comes from the layer within which the outlet lies until a critical flow rate is reached, above which flow from nearby layers begins. Experiments provide a range of different critical values and flow patterns depending on the geometry, density, type of withdrawal (line or point), flow rate, initial configuration and a range of other factors [3–8].

Theoretical work has usually been restricted to the study of a single fluid layer with a free surface, for which the steady equations are identical provided the interface is very thin, the upper fluid is assumed to be stagnant and gravity, g , is replaced by a reduced gravity

(moderated by the density difference), i.e., $g' = (\Delta\rho/\rho)g$, where $\Delta\rho$ is the density difference and ρ is some reference density, see e.g. [9, 10].

These steady solutions have been described in a range of papers and consist of two major types; cusp-like solutions [11–15], [8] in which the free surface is drawn down into a cusp above the sink, and stagnation point flows [16, 17, 13, 15] in which it rises to a single stagnation point above the sink. Steady supercritical flows, in which both layers are flowing, have been obtained quite recently in a series of papers, [9, 10, 18]. Almost all conclusions on critical drawdown values resulting from this work have been speculative.

Unsteady solutions have been described in papers by Tyvand *et al.* [19] (small time expansion) and for the case of a point sink in Xue and Yue [20] (numerical), and Miloh and Tyvand [21] (numerical and small time). These authors compute the initial motion of the free surface of a single layer of fluid in various configurations of depth.

The particular problem to be considered in this paper is perhaps the simplest (and most idealised) of all withdrawal configurations, in which a line sink situated beneath a free surface withdraws an inviscid, incompressible fluid.

The main parameter that defines such flows is the Froude number

$$F = \left(\frac{m^2}{4\pi^2 g H^3} \right)^{1/2}, \quad (1)$$

where m is the sink strength, H is the sink depth beneath the undisturbed free surface and g is gravitational acceleration. Current research on this problem seems to indicate that at low flow rates, steady stagnation point flows exist, and these have been obtained up to $F = 0.23$. No solutions have been obtained for the range of F from this value up to $F = 0.56$ where a unique, steady, cusped solution exists (see [13]). Above this value, no further solutions have been obtained, but if we allow the presence of a second, lighter fluid above, Hocking [10] showed that two-layer flows seem to occur for $F > 0.56$. This suggests that in the steady configuration at least, $F = 0.56$ is the maximum value at which single layer steady flows exist, and above this value the flow is two-layer with a shallower angle of entry of the interface into the sink as F increases.

It is the aim of this paper to investigate this process more deeply using both theoretical and numerical techniques to analyse the unsteady flow. A small-time expansion will be derived for two cases of relevance to the withdrawal from a line sink submerged beneath a free surface (air-water interface). This part of the work is similar to that of Tyvand [19], although we consider two situations each with different initial condition to that used in [19], and we shall argue our approach is correct. This is followed by some numerical simulations of the same events, that are used to explore possible drawdowns and movement to steady states.

Evidence will be given to suggest that there are two critical values of the Froude number. One of these is related to the initiation of the flow and the other to the case of a fully developed flow with slowly increasing Froude number, such as when the water level is slowly dropping. These results help to explain the diversity in critical values obtained in experiments. To obtain clear results it was found necessary to introduce some surface tension. Results will be compared with known steady solutions (see [33]) and discussed in context.

2. Problem formulation

In this paper we consider the unsteady, irrotational flow of an inviscid, incompressible fluid into a line sink beneath a free surface. The line sink is initially at a depth H (m) beneath the

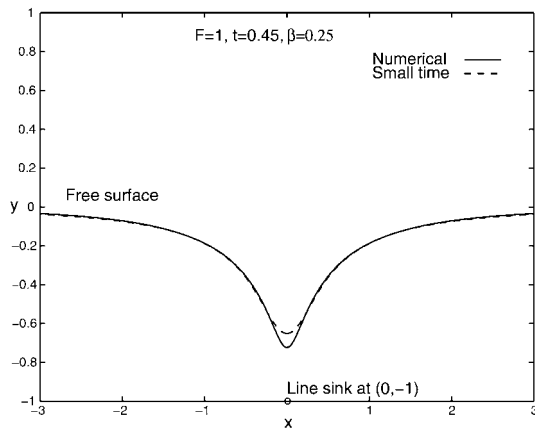


Figure 1. Two free surface plots obtained by different methods.

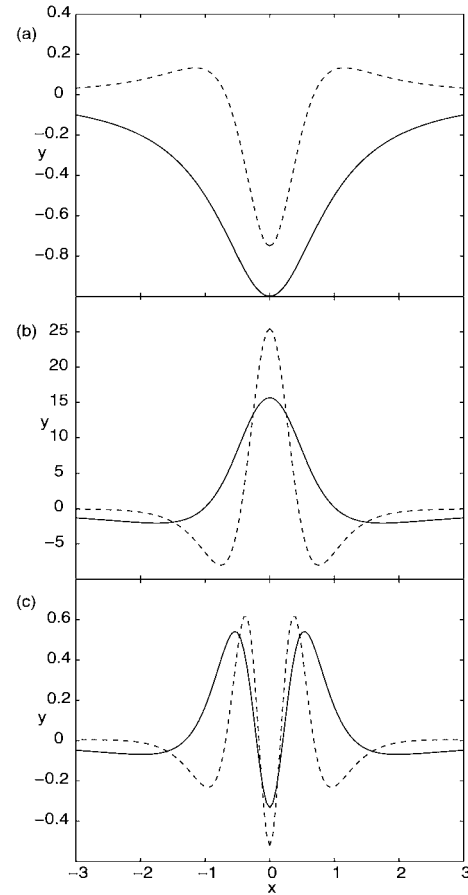


Figure 2. (a) η_1 (solid) and η_2 (dashed) terms, single-sink case; (b) η_3 (solid) and η_4 (dashed) terms, single sink case for $F = 0.1$ and $\beta = 0$; (c) η_3 (solid) and η_4 (dashed) terms, single-sink case for $F = 0.5$ and $\beta = 0$.

undisturbed level of the free surface and has strength m (m^2/s per unit width) that is not always constant. The free surface is assumed to have surface tension S , although often this will be set to zero. Figure 1 shows the flow configuration and the results of two calculations of free surface shapes.

The consequences of these assumptions are that we can define a velocity potential $\Phi(\hat{x}, \hat{y}, \tau)$ such that $\hat{\mathbf{u}} = \nabla \Phi$ is the velocity vector for the flow and satisfies

$$\nabla^2 \Phi = 0, \quad \hat{y} < N(\hat{x}, \tau) \quad (2)$$

throughout the fluid domain except at the point $\hat{\mathbf{x}} = (0, -H)$, the location of the line sink, and where $\hat{y} = N(\hat{x}, \tau)$ is the equation of the free surface. As the line sink is approached, the velocity potential satisfies

$$\Phi \rightarrow -\frac{m}{2\pi} \log \sqrt{\hat{x}^2 + (\hat{y} + H)^2} \quad \text{as} \quad (\hat{x}, \hat{y}) \rightarrow (0, -H). \quad (3)$$

In addition, there are the dynamic condition that enforces the condition of atmospheric pressure at the surface, *i.e.*,

$$\Phi_\tau + \frac{1}{2}(\hat{u}^2 + \hat{v}^2) + gN + \frac{SN_{\hat{x}\hat{x}}}{(1 + N_{\hat{x}}^2)^{3/2}} = 0, \quad \text{on} \quad \hat{y} = N(\hat{x}, \tau) \quad (4)$$

and the kinematic condition, *i.e.*,

$$N_\tau + \Phi_{\hat{x}}N_{\hat{x}} - \Phi_{\hat{y}} = 0 \quad \text{on} \quad \hat{y} = N(\hat{x}, \tau). \quad (5)$$

Finally, there are the conditions that $\hat{\nabla}\Phi \rightarrow 0$ and $N \rightarrow 0$ as $(\hat{x}, \hat{y}) \rightarrow \infty$, *i.e.*, the velocity must vanish and the free surface must approach the stagnation level at a large distance from the sink.

To reduce the number of parameters we non-dimensionalise with respect to the potential $\Phi = (m/2\pi)\phi$, the time scale $\tau = (2\pi H^2/m)t$ and the length scales $\hat{x} = Hx$, $\hat{y} = Hy$. Thus, the non-dimensional equations are

$$\nabla^2\phi = 0, \quad y < \eta(x, t), \quad \mathbf{x} \neq (0, -1), \quad (6)$$

subject to

$$\phi_t + \frac{1}{2}(u^2 + v^2) + F^{-2}\eta + \frac{F^{-2}\beta\eta_{xx}}{(1 + \eta_x^2)^{3/2}} = 0 \quad \text{on} \quad y = \eta(x, t) \quad (7)$$

and

$$\eta_t + \phi_x\eta_x - \phi_y = 0 \quad \text{on} \quad y = \eta(x, t), \quad (8)$$

with the extra condition that

$$\phi \rightarrow -\log \sqrt{x^2 + (y + 1)^2} \quad \text{as} \quad (x, y) \rightarrow (0, -1), \quad (9)$$

since the sink is situated at $y = -1$ in the new system, and $y = \eta(x, t)$ is the location of the free surface. The important quantities are then the Froude number and the nondimensional surface tension,

$$\beta = \left(\frac{S}{gH^2} \right). \quad (10)$$

Sometimes we will assume the presence of an image sink at $(0, 1)$ of equal strength to the submerged sink, since this alters the initial condition of the problem to one in which all vertical velocities along the free surface are assumed to be zero initially. This represents a perturbation to an established flow from a non-impulsive start, and provides useful information about drawdowns and movement to steady states from a gradual start. In this situation then, we have

$$\phi \rightarrow -\log \sqrt{x^2 + (y - 1)^2} \quad \text{as} \quad (x, y) \rightarrow (0, 1). \quad (11)$$

3. Small-time expansions

In this section we compute the small time expansions for two situations involving a submerged sink beneath a free surface including surface tension. The single sink case has a sink beneath

the surface at $(0, -1)$, while the two sink case has an image sink situated at $(0, 1)$ outside of the fluid domain. We contrast our approach with that of Tyvand [19], in which an image of equal magnitude and opposite direction to the submerged sink is assumed present.

3.1. INITIAL CONDITIONS

The reason for studying the two different problems is provided by a careful consideration of initial conditions appropriate to withdrawal flows. Tyvand [19] argues that the correct condition is that the potential should have the value $\phi(x, 0, 0) = 0$; that the potential is constant on the free surface at the moment the sink is initiated. To ensure this condition is satisfied requires the addition of an image source, and effectively imposes a downward velocity at the surface at $t = 0$ at around double the velocity induced by a single sink and not toward it.

On the other hand, we argue that when the sink is initiated the fluid behaves as if there is no free surface, *i.e.*, feels the direct impact of the potential due to the single sink before rebounding due to gravity. This is consistent with the fact that gravity does not appear until the third term in the small time expansion, and also with the initial conditions assumed in the stratified-flow literature (see *e.g.* Yih, [2]).

The problem involving an image sink enforces a condition that the vertical velocity is zero on the free surface at the initial time. This is like placing a rigid lid on the free surface, letting the flow develop, and then instantaneously removing the lid. This generates a response that we show later to be very similar to the response of a sink that is turned on very slowly.

3.2. SERIES SOLUTION IN THE GENERAL CASE

Small-time expansions for each of the cases were considered up to fifth order in time t about the undisturbed surface level $y = 0$. These expansions took the form

$$\eta(x, t) = \eta_1(x)t + \eta_2(x)t^2 + \dots + \eta_5(x)t^5, \quad (12)$$

$$\phi(x, y, t) = \phi_0(x, y) + t\phi_1 + t^2\phi_2 + \dots \quad (13)$$

Details are given in the appendix. For the case of a single sink, we obtained the first four terms, whereas for the image sink case we went up to order 5, because $\eta_1(x) = 0$ in that case, and the Froude number F and the surface-tension coefficient β do not make an appearance until the fourth order (compared to the third order term in the single sink case).

3.3. SINGLE-SINK CASE

Here we assume

$$\phi_0(x, y) = -\frac{1}{2} \log(x^2 + (y + 1)^2), \quad (14)$$

representing a sink immersed in the fluid at $(0, -1)$ that is turned on at $t = 0$. (Recall that the fluid free surface is at $y = 0$ initially.) From the first kinematic condition (A9), given in the appendix, we obtain

$$\eta_1(x) = \phi_{0y} = -\frac{1}{x^2 + 1}. \quad (15)$$

Using the first-order dynamic condition from (A7) as in the appendix, along with symbolic differentiation and substitution in *Maple*, we obtain

$$\phi_1(x, 0) = -\frac{1}{2}(\phi_{0x}^2 + \phi_{0y}^2) = -\frac{1}{2} \frac{1}{(x^2 + 1)}. \quad (16)$$

Laplace's equation is solved using *Maple*, as described in the appendix, to obtain the complex potential function $w_1(z) = -\frac{1}{2(z-i)}$, where $z = x + iy$, so that

$$\phi_1(x, y) = \Im(w_1(x + iy)) = \frac{y - 1}{2(x^2 + (y - 1)^2)}. \quad (17)$$

From (A10) in the appendix we then obtain

$$\eta_2 = \frac{1}{2}(\phi_{1y} + \eta_1 \phi_{0x}^2 - \eta_{1x} \phi_{0x}) = \frac{x^4 + 6x^2 - 3}{4(x^2 + 1)^3}, \quad (18)$$

while from the dynamic condition (A8) in the appendix,

$$\begin{aligned} \phi_2(x, 0) &= -\frac{1}{2} \left(\phi_{0x}(\phi_{1x} + \eta_1 \phi_{0yx}) + \phi_{0y}(\phi_{1y} + \eta_1 \phi_{0yy}) + \eta_1(\phi_{1y} + F^{-2}) - \beta \frac{\eta_{1xx}}{F^2} \right) \\ &= \frac{x^2 - 1}{(x^2 + 1)^3} + \frac{1}{2F^2(x^2 + 1)} + \beta \frac{1 - 3x^2}{F^2(x^2 + 1)^3}. \end{aligned}$$

Computing the complex potential function gives

$$w_2(z) = \frac{1 + \frac{3i}{4}z - \frac{1}{4}z^2}{(z - i)^3} + \frac{1}{2F^2(z - i)} - \frac{\beta}{F^2(z - i)^3}, \quad (19)$$

and so, with $\phi_2(x, y)$ the imaginary part of $w_2(z)$, the kinematic condition (A11) in the appendix gives

$$\begin{aligned} \eta_3 &= -\frac{1}{3} \left(\eta_1(\eta_1 \phi_{0yx} + \phi_{1x}) - \eta_1 \phi_{1yy} + \eta_{2x} \phi_{0x} - \frac{1}{2} \eta_1^2 \phi_{0yyy} - \eta_2 \phi_{0yy} - \phi_{2y} \right) \\ &= \frac{(x^8 - x^6 - 5x^4 + 81x^2 - 12)}{12(x^2 + 1)^5} - \frac{1}{6F^2} \frac{(x^2 - 1)}{(x^2 + 1)^2} + \frac{\beta}{F^2} \frac{(x^4 - 6x^2 + 1)}{(x^2 + 1)^4}. \end{aligned}$$

The third-order dynamic condition now gives $\phi_3(x, 0)$ and hence a potential function $w_3(z)$. From this, the imaginary component $\phi_3(x, y)$ is then obtained. (The details are tedious and so are omitted.) The fourth-order kinematic condition then gives

$$\begin{aligned} \eta_4 &= \frac{(-77 + 1075x^2 - 914x^4 - 70x^6 + 91x^8 + 19x^{10} + 4x^{12})}{48(x^2 + 1)^7} \\ &\quad - \frac{1}{F^2} \frac{(-13 + 71x^2 - 11x^4 + x^6)}{48(x^2 + 1)^4} \\ &\quad - \frac{\beta}{F^2} \frac{(-113 + 1773x^2 - 1874x^4 + 82x^6 + 3x^8 + x^{10})}{32(x^2 + 1)^6}. \end{aligned}$$

3.4. IMAGE-SINK CASE

Here, the process is identical to the one sink case except that the initial potential function (14) is replaced by

$$\phi_0(x, y) = -\frac{1}{2} (\log(x^2 + (y+1)^2) + \log(x^2 + (y-1)^2)), \quad (20)$$

which adds an image sink at $(0, 1)$, outside of the fluid domain.

Following the same procedure as for the single sink case, we successively calculate: $\eta_1(x) = \phi_{0,y} = 0$, $\phi_1(x, 0) = -2/(x^2 + 1)$ and hence

$$\phi_1(x, y) = \frac{x^2y - 2x^2 + y^3 - 2y^2 + y}{(x^2 + (y-1)^2)^2}. \quad (21)$$

Then, we obtain

$$\eta_2 = \frac{x^4 - 6x^2 + 1}{2(x^2 + 1)^3}, \quad (22)$$

and $\phi_2(x, 0) = \frac{4x^2(x^2-1)}{(x^2+1)^4}$, so

$$\phi_2(x, y) = \frac{4x^4 - 3x^4y - 4x^2y^2 + 8x^2y - 4x^2 + y^5}{(x^2 + (y-1)^2)^4}, \quad (23)$$

and

$$\eta_3 = \frac{-6x^6 + 72x^4 - 49x^2 + 1}{3(x^2 + 1)^5}. \quad (24)$$

Again, the calculation of ϕ_3 becomes very involved and is omitted, but we can go on to obtain

$$\begin{aligned} \eta_4 = & \left(\frac{28 - 2471x^2 + 11189x^4 - 7350x^6 + 478x^8 + 13x^{10} + x^{12}}{48(x^2 + 1)^7} \right) \\ & + \frac{1}{F^2} \left(\frac{-3x^8 + 2x^6 + 12x^4 + 6x^2 - 1}{6(x^2 + 1)^6} \right) + \frac{\beta}{F^2} \left(\frac{60x^6 - 480x^4 + 396x^2 - 24}{6(x^2 + 1)^6} \right), \end{aligned}$$

and, this time continuing to fifth order,

$$\begin{aligned} \eta_5 = & \frac{1}{3840(x^2 + 1)^9} (-11x^{16} - 324x^{14} - 5556x^{12} - 189460x^{10} \\ & + 3770334x^8 - 9368044x^6 + 5046892x^4 - 504636x^2 + 245) \\ & - \frac{1}{960F^2(x^2 + 1)^6} (5x^{10} + 21x^8 - 4494x^6 + 20874x^4 - 10119x^2 + 337) \\ & - \frac{\beta}{160F^2(x^2 + 1)^8} (3x^{14} + x^{13} + 15x^{12} + 6x^{11} + 27x^{10} \\ & - 2593x^9 + 8975x^8 + 15700x^7 - 101135x^6 + 623x^5 + 144101x^4 \\ & - 15290x^3 - 32015x^2 + 2385x + 509). \end{aligned}$$

3.5. ANALYSIS OF THE SINGLE-SINK CASE

We begin by observing that neither F nor β appear in the functions η_1 , η_2 in equations (15), (18). Therefore, neither gravity nor surface tension plays a role in the initial flow that results

from turning on the sink. Figure 2(a) shows these two functions; the solid line represents $\eta_1(x)$ and $\eta_2(x)$ is drawn with a dashed line. Each of the first two terms has the effect of causing a dip in the free surface centred on $x = 0$. However, for some values of F and β , the higher-order functions η_3 and η_4 represent dips, and for other values they represent swells.

Figure 2(b) shows η_3 and η_4 for $F = 0.1$ and $\beta = 0$, while in Figure 2(c), these same two functions are plotted for parameters $F = 0.5$ and $\beta = 0$. Thus for $F = 0.1$, after the initial dip due to the order 1 and 2 terms, there will be a tendency to bounce back due to the next two terms. However, for $F = 0.5$, the initial dip is reinforced and one might expect the dip to continue to travel downward.

A separate consideration of the component of the expansion due to non-zero surface tension is of interest. Plots of the terms involving β in η_3 and η_4 (not shown) indicate that as surface tension increases, any tendency of the initial downward motion of the point at $x = 0$ to reverse its downward motion due to η_1 and η_2 is accentuated.

Overall then, for those values of F and β for which η_3 (and η_4 , which changes behaviour in step with η_3) has a positive local maximum at $x = 0$, there will be a tendency for that point to reverse direction after its initial descent, whereas if η_3 has a negative local minimum at $x = 0$, the initial descent will be accentuated and the $x = 0$ point can be expected to continue its descent until $y = -1$ and the submerged sink is reached. In [19] it is reasoned that the sign at $x = 0$ of the third order term η_3 will determine closely whether the surface descends to the sink or not, and that higher-order terms are unlikely to influence this greatly. However, as we see shortly, this only provides a rough guide; certainly if η_3 has a dip, drawdown takes place, but the opposite is not true. Hence only a crude upper bound on the critical Froude number for drawdown can be obtained by examining where $\eta_3(0)$ changes sign. Moreover, this upper bound worsens as surface tension β increases, because the time to drawdown increases.

Nevertheless, we now consider these sign changes and obtain the upper bounds. Considering first the case of η_3 , we have that $\eta_3(0) = \frac{1+6\beta}{6F^2} - 1$, which is zero when $F = \sqrt{\frac{1}{6} + \beta}$. For $\eta_4(0) = -\frac{77}{48} + \frac{26+339\beta}{96F^2}$ to be zero, we require $F = \sqrt{\frac{339\beta+26}{154}}$. In both cases, if F is greater than the given value, the term represents a dip, and if it is less, a hump occurs. Plots of the two functions of β are given in Figure 3 (dashed lines), and are compared with values obtained by numerical simulations (solid line), which we discuss later. Once the fourth term also contains a dip, both the third and fourth terms are driving the fluid downward and drawdown seems inevitable, especially as the Froude number is effectively increased as the free surface approaches the sink.

At the other end of the scale, when F is very small, say 0.01 or less, the time taken to move to the initial minimum at $x = 0$ is itself very small, and more reliance can be placed on predictions from the small time expansion. From Equation (12) we have

$$\eta(0, t) = -t - \frac{3}{4}t^2 + \left(\left(\frac{1}{6} + \beta \right) / F^2 - 1 \right) t^3 + \left(\frac{339\beta + 26}{96F^2} - \frac{77}{48} \right) t^4. \quad (25)$$

Now making the substitutions $s = t/F$ and $Y = \eta(0, t)/F$ gives the scaled surface elevation at $x = 0$ in the form

$$Y(s) = -s - \frac{3}{4}Fs^2 + \left(\frac{1}{6} + \beta \right) - F^2s^3 + \dots \quad (26)$$

As $F \rightarrow 0$, this third-order polynomial can be shown, using standard calculus procedures, to have a local minimum $Y_{\min} = -(\frac{2}{3})/\sqrt{\frac{1}{2} + 3\beta}$ at $s = 1/\sqrt{\frac{1}{2} + 3\beta}$, and so, in terms of the

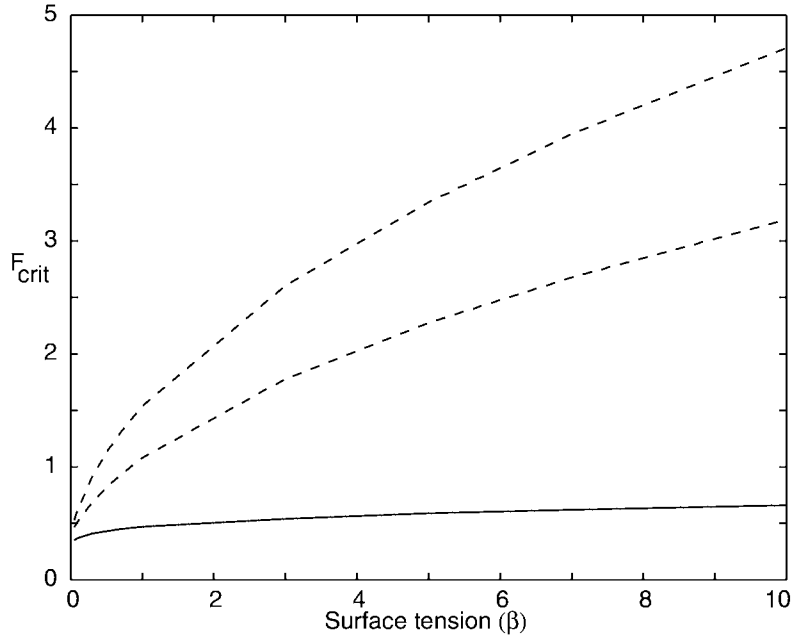


Figure 3. Critical F against β , single-sink case: from simulations (solid) and from setting $\eta_3(0) = 0$ (lower dashed) and $\eta_4(0) = 0$ (upper dashed).

original variables, there is a local minimum $\eta_{\min} = -(\frac{2F}{3})/\sqrt{\frac{1}{2} + 3\beta}$ at time $t = F/\sqrt{\frac{1}{2} + 3\beta}$ in the surface elevation at $x = 0$, for $F \rightarrow 0$. Thus the magnitude of η_{\min} decreases as $F \rightarrow 0$, and also as $\beta \rightarrow \infty$.

Once the minimum is achieved, the small time expansion suggests the dip rebounds. In practice, a wave can be expected, with oscillations of amplitude comparable in size to the initial dip. A comparison with the known steady-state solution $\eta_s(x) = \frac{-2F^2x^2}{(x^2+1)^2}$ in [17] (which is accurate to second order in F) is of interest here. Note that $\eta_s(x)$ is directly proportional to F^2 , whereas the forecast minimum value of $\eta(0, t)$ is directly proportional to F . This suggests that even for small F , the steady state surface shape is unlikely to be reached very quickly, with oscillations instead being an order of magnitude larger than the depth of the steady state dip. This is in contrast with the speculation in [19] that for small F a steady state may be obtained. While it is possible that the free surface will eventually reach a steady state, it is well beyond the scope of this small-time expansion to determine this. Thus it appears that the wave motion due to the impulsive start drowns out the tendency to move to a steady state.

3.6. ANALYSIS OF THE IMAGE-SINK CASE

This approach was of interest because it can be argued that it models an established flow situation rather than an impulsive start such as in the single-sink case above. Thus the flow due to a sink that was turned on with a very low flux and then slowly increased in strength might evolve to a situation resembling this. Equivalently, the flow with a sink situated a long way beneath the free surface might evolve to this as the level of the surface drops. Tests of the former of these using the numerical method described in the next section give credence to this argument. Thus using this formulation we are able to consider asymptotically the behaviour of

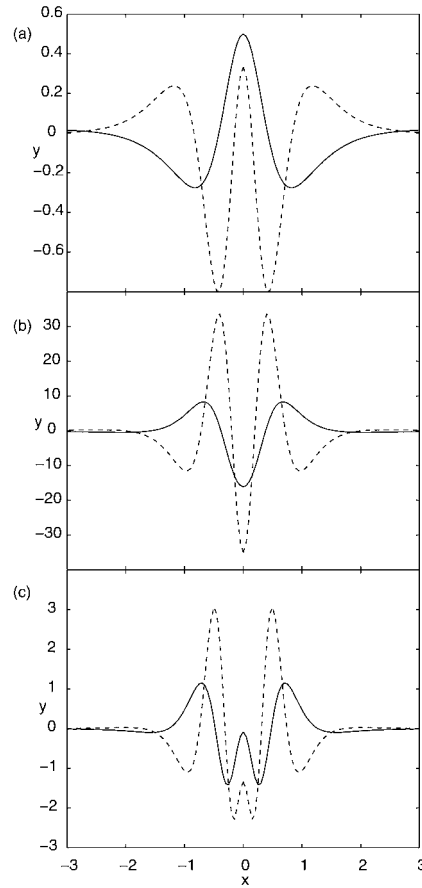


Figure 4. (a) η_2 (solid) and η_3 (dashed), image-sink case, (b) η_4 (solid) and η_5 (dashed) for $F = 0.1$ with $\beta = 0$; (c) η_4 (solid) and η_5 (dashed) for $F = 0.5$ with $\beta = 0$.

an ‘established’ flow. Comparisons can then be made with steady state computations existing in the literature, see *e.g.* [12, 22, 14, 17, 16, 11, 13, 15].

For this case, $\eta_1(x) = 0$, and neither F nor β make an appearance until the fourth order coefficient. The second and third order coefficients are plotted in Figure 4(a), and the fourth and fifth in (b) and (c) for $F = 0.1$, $\beta = 0$, and $F = 0.5$, $\beta = 0$, respectively. Note that η_2 and η_3 represent swells or crests, that is they possess positive local maxima at $x = 0$, and are mitigated by both η_4 and η_5 for small F , but less so for larger F . However, the first three non-zero terms have a dip on either side of the central swell and it is this which turns out to be of greatest interest in terms of the drawdown.

Introducing non-zero surface tension coefficient β produces (as in the single-sink case) an effect in opposition to whatever motion occurs in the zero-surface-tension case, thus reducing the magnitude of any events.

For small F we can again consider the size of the initial swell at $x = 0$. From Equation (12) we have

$$\eta(0, t) = \frac{1}{2}t^2 + \frac{1}{3}t^3 + \left(\frac{28}{48} - \frac{1}{F^2}\left(\frac{1}{6} + 4\beta\right)\right)t^4 + \dots \quad (27)$$

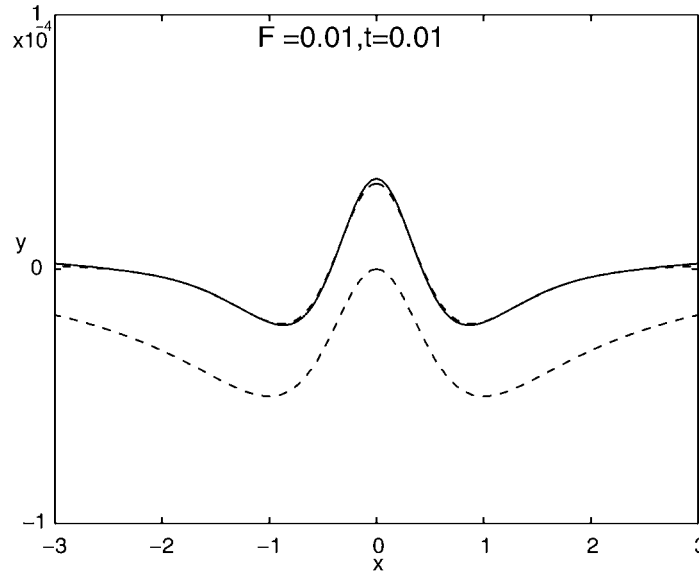


Figure 5. Comparison of the image-sink small-time (upper dashed) and numerical (solid) solutions with the steady state (lower dashed), with $F = 0.01$, at $t = 0.01$.

Here, we make the substitutions $s = t/F$ and $Y = \eta(0, t)/F^2$ and obtain, in the limit $F \rightarrow 0$, $Y(s) = \frac{1}{2}s^2 - (\frac{1}{6} + 4\beta)s^4 + \dots$. This fourth-order polynomial is easily shown to have a local maximum $Y_{\max} = \frac{3}{8(24\beta+1)}$ when $s = \sqrt{3/(48\beta+2)}$. Thus the surface at $x = 0$ has a maximum height

$$\eta_{\max} = \frac{3F^2}{8(24\beta+1)} \quad \text{at time } t = F\sqrt{\frac{3}{48\beta+2}}.$$

This is clearly directly proportional to F^2 instead of to F itself, and the surface-tension coefficient is no longer under a square root, but again non-zero surface tension acts to reduce the size of the disturbance relative to the zero-surface-tension case. These results are consistent with the size of the known steady-state stagnation-point solutions, [22, 17, 16].

In fact for small F and various β up to around 2 (where the amplitude of the initial swell is already greatly reduced), the small-time expansion does resemble the steady state briefly, albeit elevated above it, before diverging as t becomes too large. However, it is difficult to draw conclusions about critical values. A plot suggests that the $F = 0.01$, $\beta = 0$ case will move towards a steady state: see Figure 5, where the free surface is shown with the steady state solution at $t = 0.01$, both dashed. The small time plot is the upper one and the solid line was obtained via a numerical simulation. The small time expansion diverges significantly from this shortly after and ceases to be valid.

At larger values of F , the situation appears more complicated. In this case, since the middle of the free surface is never pulled downward, the collapse of the free surface into the sink would correspond to the dips either side of the point $x = 0$ being pulled down and inward and a central cigar shape pinching off in the middle. Numerical simulations will later confirm this behaviour. This suggests that the behaviour at $x = 0$ is no longer a crucial factor.

Both η_2 and η_3 have positive local maxima at $x = 0$. Hence, arguing as in the single-sink case, a possible guide to the critical Froude number for pinch-off to occur is the sign of $\eta_4(0)$. From *Maple*, $\eta_4(0)$ changes from negative to positive when

$$F = \sqrt{\frac{2 + 48\beta}{7}}.$$

Perhaps pinching off occurs above this value, $F = 0.5345$ when $\beta = 0$. This compares with the unique value of Froude number, $F = 0.567$, at which a cusp solution occurs, [13]. We might expect that for F above this drawdown would occur.

4. The numerical method

In order to compare with these results and to gain a picture of what is happening for larger times we performed a series of numerical simulations. Our approach was similar to that used by Tuck amongst others (see [23] and [24]). It is a semi-Lagrangian approach in which we follow the evolution of points on the free surface subject to an evolving flux. We use a recursive process to update the global velocity potential and the positions of N points on the free surface at each time step.

Initially, we assume the sample points are at rest and in some fixed positions $(X_i^{(0)}, Y_i^{(0)})$ along the free surface, and impose an instantaneous velocity potential function $\phi^{(0)}(x, y)$, that may be identically zero or may assume the presence of some sources or sinks. In practice, the points are assumed to be symmetrically distributed about the y -axis and all sources and sinks generating the flux were likewise assumed to be symmetrically distributed both spatially and in terms of strength.

The recursive step modifies each point's position and the value of the potential function at each point and hence everywhere (by solving the Dirichlet problem). Thus if at time step t , the i 'th point has coordinates $(X_i^{(t)}, Y_i^{(t)})$ and the global velocity potential is $\phi^{(t)}(x, y)$ at all points (x, y) in the fluid, so that $\Phi_i^{(t)} = \phi_t(X_i^{(t)}, Y_i^{(t)})$, the velocity potential at the i 'th point, then the three equations determining the time evolution of all points are (dropping the time superscript for simplicity):

$$\frac{dX_i}{dt} = u_i \tag{28}$$

$$\frac{dY_i}{dt} = v_i \tag{29}$$

$$\frac{d\Phi_i}{dt} = \frac{1}{2}((u_i)^2 + (v_i)^2) - F^{-2}(Y_i - \beta T_i). \tag{30}$$

Here $u_i = \phi_x(X_i, Y_i)$ and $v_i = \phi_y(X_i, Y_i)$, and T_i is a surface tension term computed numerically from the current set of free-surface points as

$$T(x) = y''/(1 + (y')^2)^{\frac{3}{2}}, \tag{31}$$

where (x, y) is on the free surface and the derivatives are with respect to x following the free surface. Finite differences were used to perform these slope and curvature calculations. Hence the values of X_i , Y_i and Φ_i can be moved forward one time step.

The task remains to determine $\phi^{(t+1)}$ from the $\Phi_i^{(t+1)}$ values just computed. To do this, we must solve a Dirichlet problem. Assume positions $P_i = (X_i, Y_i)$ for the N free surface points at time step t , and values Φ_i for ϕ given at each. Choose the source point (x_i, y_i) just ‘above’ the free-surface point (X_i, Y_i) and approximately normal to the surface. (The exact means of determination in order to optimise the numerical performance is discussed later.) Let $R_i(x, y) = \sqrt{(x - x_i)^2 + (y - y_i)^2}$, the distance between the i ’th source and the point (x, y) , and let $R_1(x, y) = \sqrt{x^2 + (y - 1)^2}$, $R_2(x, y) = \sqrt{x^2 + (y + 1)^2}$, the distances between (x, y) and the sinks one unit above and below the origin, respectively. We assume a solution of the form

$$\phi(x, y) = \sum_{i=1}^N q_i \log R_i + s_1 \log R_1 + s_2 \log R_2. \quad (32)$$

It is always the case that $s_2 = -1$ while s_1 is either 0 or -1 . The source strengths q_i are unknown constants which are determined once the values of ϕ are given at N distinct points. Thus we obtain N linear equations in the q_i of the form

$$\Phi_j = \sum_{i=1}^N q_i \log R_i(X_j, Y_j) + s_1 \log R_1(X_j, Y_j) + s_2 \log R_2(X_j, Y_j) \quad (33)$$

and solve to give ϕ , and hence $u = \phi_x$ and $v = \phi_y$, at time step $t + 1$.

In practice, the symmetry assumption almost halves the number of q_i to be determined, with points to the right of the y -axis being matched up with points to the left.

The far-field condition of zero total flux was enforced by resetting the outermost value of y to zero and adjusting all other y values by the same quantity. This makes less and less difference the more points that are used and the further out the x -values go before truncation.

4.1. THE STARTING POINTS

In order that run time was not prohibitive, a limit on the number of points placed along the initial free surface was necessary. Following [23] and [24], we chose the points nearest the origin to be equally spaced, with a geometrical increase in the spatial increment beyond that. Generally, a third of the points were chosen to be equally spaced, the remaining outer points spreading apart at a ratio of r , usually $r = 1.1$. A problem during long runs was the spurious numerical reflection of information at the truncation point of the infinite domain. In general, this problem was overcome by moving the truncation point further out and using more points.

The number of points needed to ensure a realistic simulation varied. For large Froude numbers, the fluid flows rapidly out through the sink and the simulation generally ceases to be valid because the surface is drawn down and the sinks (x_i, y_i) move inside the fluid. This means fewer points are required since the chance of numerical reflections from the truncation point is lower. For smaller Froude numbers, however, reflections were a factor and more points were needed.

4.2. SOURCE POSITIONS AND THE USE OF SPLINES

At any given iteration the point positions define the free-surface shape. The problem from this point is to choose source locations (x_i, y_i) that are outside the fluid but close enough to it to give a good approximation to the global potential function $\phi(x, y)$ in the next round, as well as

to ensure the sources are outside the flow domain even if the surface becomes quite distorted. On the other hand, a choice too close to the surface may lead to numerical instabilities. Based on trial and error, a value of 0.025 was used for the separation distance in most simulations. We chose the source point location $S_i = (x_i, y_i)$ so that the segment from it to $P_i = (X_i, Y_i)$ bisected the angle between the segments from P_{i-1} to P_i and from P_i to P_{i+1} , a distance 0.025 from P_i .

In longer runs, the drift of free-surface points toward $x = 0$ due to the sink flow tended to cause compression of the points and consequently numerical instabilities sometimes developed. In addition, points further out were often drawn inward leaving insufficient points to resolve the outer region. In such cases cubic-spline interpolation was used to re-position points along the free surface. This was done immediately after calculation of the new free-surface-point positions and the new global potential function. The free-surface points became the basis of the spline interpolation, and then the freshly calculated global potential function was used to re-compute the Φ_i at the re-positioned points, for the next round of computations. Using arc-length as a parameter (or more strictly, point number), we could apply splines, even if the free surface ceased to be describable as a function $Y = f(X)$. Simulations using this process ran for much longer than those without re-positioning.

5. Results of numerical experiments

We used Fortran77 to generate all simulations and then viewed the results using *Matlab*. The result was a series of ‘movies’ of the evolution of the free surface. Some experimentation with the parameters was necessary to ensure a stable numerical scheme. However, in most cases the combination of widening the computation domain and using smaller time steps was sufficient to ensure reliable simulations.

A common cause of termination of simulations was a breaking wave, after which the free surface was no longer well-defined and in particular the source points used to define the evolving flux function would move inside the fluid and the output would become meaningless. Also, simulations with non-zero surface tension required a much smaller time step due to the second derivative term in the numerator of the surface tension term, (31).

Throughout, δt , δx , N , r , x_{\max} and d denote the time increment used, the initial space increment along the x -axis between successive points, the number of points used (to the right of the y -axis plus the one at the origin), the multiplying factor for the spatial increment after the first $N/3$ points have been spaced equally, the initial x -coordinate of the outermost point (determined by δx , N and r) and the distance ‘above’ the free surface points of the corresponding source points. Unless stated otherwise, the following values apply: $\delta x = 0.05$, $N = 120$, $r = 1.1$, $x_{\max} \approx 85$, d equal to twice the local grid spacing. Larger values of N did not appear to noticeably alter the results. The x -increment size around $x = 0$ of $\delta x = 0.05$ seemed to be an optimal compromise between avoiding numerical instability and having sufficient points to obtain converged solutions.

5.1. SINGLE-SINK CASE

The free surface was initially pulled down everywhere (for all F and β) with the middle point at $x = 0$ moving fastest. If F was large enough, this continued until drawdown occurred. If F was smaller, the central region rebounded upward relative to the rest, causing a central swell.

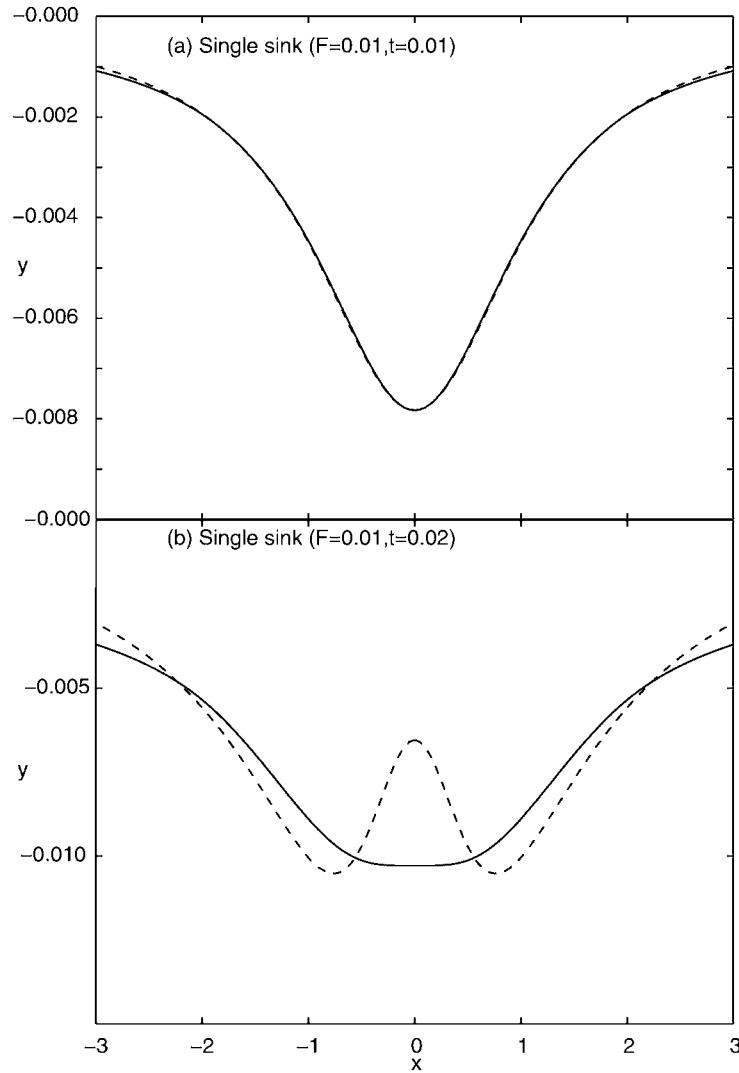


Figure 6. Small time (dashed) and numerically computed (solid) free-surface shapes for the single-sink case with $\beta = 0$ and $F = 0.01$: (a) $t = 0.01$, (b) $t = 0.02$.

In that case, the ‘rebound’ sometimes preceded movement to a steady state, broke down due to small breaking waves (see above), or the rebound reversed leading to drawdown.

As expected, there was good agreement with the small time approach for a wide range of values of F and β in the early stages of the simulation. Figures 6(a) and (b) show the free surface shapes obtained using the numerical (solid line) and small time solutions (dashed), with $F = 0.01$ and $\beta = 0$, at times $t = 0.01$ and $t = 0.02$, respectively. The small time expansion follows closely until the bounce-back point is reached, after which the two start to diverge. This is a fairly typical comparison, with the timing of the bounce agreeing well with the numerical results, especially for small F when rebound occurs quite soon after initiation of the flow.

The general behaviour described above was not always easy to quantify. However, for $\beta \geq 0.25$ approximately, there is a clear value of F_{crit} above which drawdown takes place and

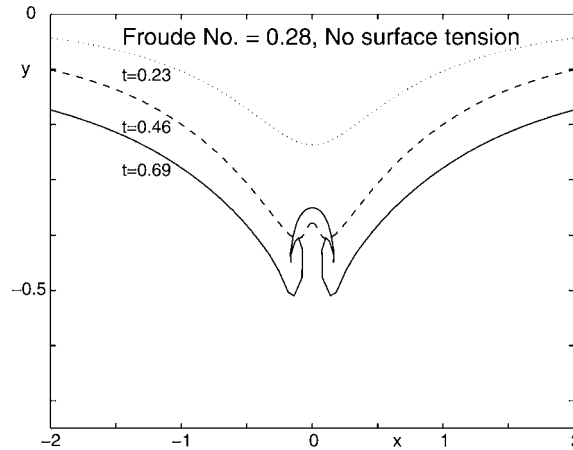


Figure 7. Numerically computed surface shapes for the single-sink case with $\beta = 0$ and $F = 0.28$, $t = 0.23, 0.46, 0.69$.

below which the simulation looks likely to move towards a steady state. (Figure 1 shows a free surface well on the way to being drawn into the sink for the case $F = 1$, $\beta = 0.25$.)

In cases with smaller β , the situation is more complicated, and indeed for $\beta \leq 0.1$, it is extremely difficult to identify a single drawdown figure. Instead, we note that the free surface can be in one of three states at the breakdown point of the simulation. In the first, the central point and indeed all points are still moving down; here it is reasonable to think that the drawdown will be direct, with the central point leading the way. In the second, the central point is moving back up at the moment of breakdown, but the lowest points are still descending, with a drawdown of the troughs to the sides of the central swell ahead of the central point appearing likely. We call this mode of drawdown *indirect*. In the third, the lowest points and central point are moving up at the moment of breakdown, with drawdown most unlikely to occur.

Figure 7 shows a simulation of a case, $F = 0.28$, for which the long term outcome is uncertain. Although the free surface is generally moving downward, there is a small section in the middle that rebounds and appears to break at around $t = 0.69$. Drawdown seemed very likely for $F = 0.38$ and even 0.30 , but not at all likely for $F = 0.24$, in which case the entire free surface between $x = -3$ and $x = 3$ was rising up away from the sink. The critical drawdown value is therefore probably somewhere between 0.25 and 0.38 .

Figure 3 shows the critical Froude numbers for drawdown at different surface tension values (solid line). In the figure, this line divides into the three F_{crit} values that divide the solution space into the three different behaviours outlined above. The middle one seems closest to a continuation of the well-defined curve for $\beta \geq 0.15$, that is, the smallest values of F for which both the central point and the sides of the central swell are still descending at the moment of breakdown of the simulation.

Note the poor match with the plots of F against β that ensure that $\eta_3(0) = 0$, and more particularly $\eta_4(0) = 0$, in the small-time expansion. Only for very small β are all of these values in relatively close agreement, suggesting that the speculation in [19] that consideration of the first few terms of the small-time expansion alone is sufficient to determine critical F for drawdown is not correct; the $\beta = 0$ case allows a rough approximation, but for $\beta > 0$ the estimates become increasingly poor. This is not surprising since the time to drawdown

increases with increasing β . At best, using the small-time expansion in this way provides a crude upper bound for the critical Froude number for drawdown.

Note that starting the surface in something other than a flat configuration did alter the observed critical value of F for drawdown. In general, the more elevated the $x = 0$ point above $y = 0$ initially, the lower the critical F -value. However, placing this point below $x = 0$ did not necessarily increase the critical Froude number.

It is also of interest to consider the possibility of evolution to a steady state. At very small F values, $F = 0.01$ say, and $\beta = 0$, travelling waves of decreasing amplitude are propagated outwards from a widening, steady central region. Consistent with the small time expansion, the magnitude of the initial movement is proportional to $0(F)$ rather than $0(F^2)$ as in the steady state. In this central region, a shape very close to that of the known steady-state solutions develops. However, due to numerical reflections from the truncation of the finite domain, as discussed above, there is a sloshing of the surface which in general increases with time eventually destroying the simulation.

Looking at larger, subcritical values of F , for instance $F = 0.20$, the simulation fails soon after the initial rebound due to the formation of breaking waves. At lower values, the simulation runs longer, with several waves propagated prior to breakdown, the steepness of these waves being the cause. The runs last progressively longer as F is made smaller, and the failure can be delayed greatly for $F \leq 0.1$ by using enough domain points. Above this value, it is impossible to predict whether an actual fluid would be likely to move to a steady state after some possible initial splashing, up to the value of $F \approx 0.23$ for which stagnation point steady states have been shown to exist, [25].

Increasing surface tension has the effect of smoothing out the small propagating waves and also reduces the tendency for the simulation to break down soon after the generation of the first wave. Consequently, steady-state solutions appear to exist for values of F closer to the critical drawdown value. Thus for instance, with $\beta = 0.25$, movement to a steady state seemed to be occurring for $F \leq 0.37$ until the spurious numerical reflections overwhelmed the computations. For this value of $\beta = 0.25$, the lowest possible value for any sort of drawdown to take place was $F = 0.38$. (By comparison, stagnation point steady states exist for $F = 0.54$ at least, as we were able to show using an iterative Newton scheme based on our unsteady code; see also [25]). Thus for $\beta \geq 0.25$, it seemed that once drawdown was averted, movement to a steady state was guaranteed. For lower values of surface tension, the situation became increasingly ambiguous; for instance, with $\beta = 0.1$, the lowest possible value of F for any possible sort of drawdown seems to be $F = 0.34$, movement to a steady state seems to happen below $F = 0.33$. This gap between drawdown and apparent movement to a steady state widens as $\beta \rightarrow 0$.

5.2. IMAGE-SINK CASE

In this case, there is an ‘imaginary’ sink one unit above the initially flat surface at $x = 0$. This provides a sink flow in which a rigid lid placed on the surface is suddenly removed. However, we suggest it also behaves like a flow that has been developing over some time with F slowly increased from zero to its final value. Apart from an increase in the magnitude of critical drawdown values and solutions that are better behaved, the overall picture of long term behaviour is similar to the single-sink case. With little or no surface tension, critical drawdown values of F are again difficult to obtain, and movement to a steady state is not observed over the full range of values where they are known to exist. However, for moderate

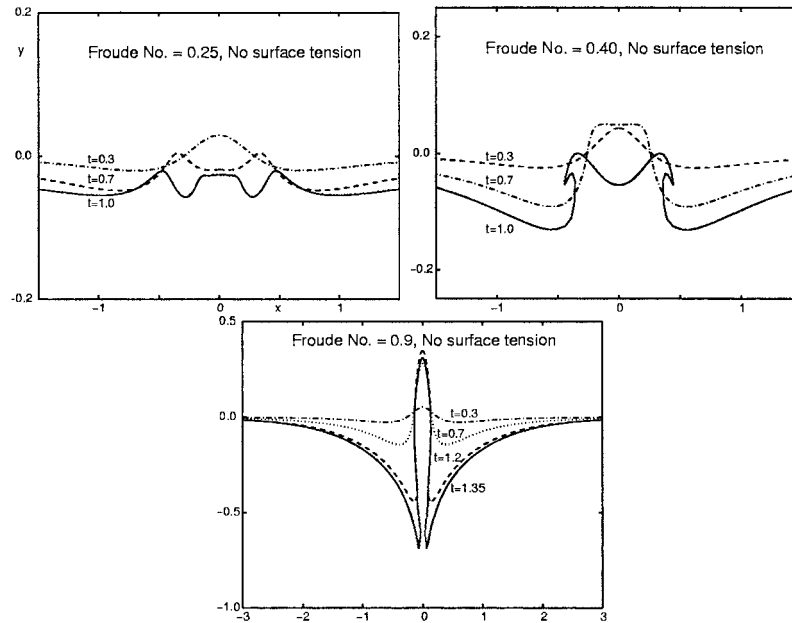


Figure 8. Numerical simulations for the two-sink case with $\beta = 0$ and (a) $F = 0.25$, (b) $F = 0.4$, (c) $F = 0.9$, at several different times.

to large β , critical values for drawdown are readily identifiable, and steady states obtained using a Newton's method based on the distributed-sink method used in this paper seem to exist right up to this critical drawdown value. Time dependent simulations seemed to verify this behaviour.

For any β and F , the middle of the free surface initially moves upward while regions either side dip down. This is followed by either breakdown of the simulation because of drawdown or a breaking wave, or by movement to a steady state. Again, there is excellent agreement with the small-time expansion at small times.

At small to moderate values of F and with $\beta = 0$, the behaviour is qualitatively similar to the single sink case. However, the amplitude of the initial disturbance is much smaller; $O(F^2)$ rather than $O(F)$. Waves are generated on the free surface above the sink and propagate outward leaving a reasonably steady central region as the amplitude of successive waves decays away eventually leading to a steady state. Figure 8(a) shows a sequence at $F = 0.25$, $\beta = 0$ in which two waves have formed and propagated outward, but show no signs of breaking. A second pair of waves has formed and propagated after the first pair.

Figure 8(b) shows a sequence with $F = 0.4$, $\beta = 0$ in which the two waves can be seen to form and propagate outwards before curling over and breaking, causing the simulation to break down.

At larger F , the middle of the free surface continues upward or stays at a steady height, while the parts either side continue to drop, resulting in the formation of a 'cigar' shape just before the dips enter the sink, see Figure 8(c), again an indirect drawdown situation. It is impossible to be definitive about the exact critical value for drawdown for $\beta = 0$, but it is possible to say that above $F = 0.7$, this indirect drawdown seems certain.

For small $\beta < 0.1$ a direct drawdown was never observed, though some form of drawdown could be inferred above some critical F . However, for $\beta \approx 0.15$, an indirect drawdown

appears likely for $F = 0.57$ (and no drawdown at all for lower F), while a direct drawdown is observed for $F > 0.7$. The size of the ‘transcritical zone’ featuring this indirect drawdown diminishes rapidly with increasing β and is all but gone for $\beta = 0.25$, the only alternatives being a direct drawdown or movement to a steady state.

As surface tension increases, so does the clarity of the picture. For $\beta = 0.02$, a case considered in [25], movement to a steady state was apparent for $F \leq 0.38$ while in [25] such steady states were shown to exist up to about $F = 0.42$, something we confirmed using Newton’s method. However, the exact value of drawdown was difficult to observe. Moving up to $\beta = 0.04$, also considered in [25], movement to steady states seemed to be occurring for $F \leq 0.45$ with drawdown appearing likely above this value. (In [25], steady states were shown to exist up to $F = 0.47$.) At this and all larger values of surface tension, there seems to be no intermediate situation in which neither drawdown nor a steady state exist.

We also performed a series of simulations in which the sink strength was increased from a smaller value of F to the value of interest. Increasing the non-dimensional sink strength is equivalent to either increasing the rate of withdrawal or the level of the surface dropping as the flow proceeds. Doing this generally produced slightly higher critical drawdown values of F , and movement to a steady state over a slightly wider range of (final) Froude numbers. Thus for example, with $\beta = 0.25$, movement to a steady state was observable for a final value of F up to 0.63 (rather than just 0.60), with drawdown seeming inevitable for $F \geq 0.64$. For much smaller β , steady states were at least observable for slightly higher F , though drawdown was still difficult to predict.

Figure 9 gives the critical drawdown value for various β ; the lower lines are the single-sink critical-value plot. The upper solid line is the smallest F for which some form of drawdown appears inevitable regardless of flow history (found using the slowly increased F and an image sink as described above). The dashed curve is the largest F for which movement to a steady state was found for any flow history (again achieved using an image sink and gradually increasing sink strength). These maximal values were confirmed to two decimal places using Newton’s method. For sufficiently large β , the two curves may well coincide if sufficient precision is used, but for quite small β , drawdowns are difficult to predict and so the drawdown curve terminates.

Thus, there is good evidence that providing surface tension is high enough, movement to a steady state is the only alternative to drawdown. Moreover, all such steady solutions can be achieved given a suitable flow history.

In [25], for $\beta = 0.02, 0.04$, it was shown that there was an interval of Froude numbers, close to the maximum Froude number for steady-state solutions, over which two steady states exist for each F . For $\beta = 0.04$, this interval was around $0.43 < F < 0.48$. With $F = 0.45$, just below the drawdown interval but within this range, evidence of both steady states was present in our simulations, though the steady state ‘above the fold’ (in the sense of [25]) was only transient. This secondary steady state has lower minimum points at the base of the central swell, and the simulation moved to a free-surface shape very similar to this, where it paused for some time before the minimal points finally started upwards to the position for the primary ‘below the fold’ steady state. For $F < 0.43$, this long pause was not observed. Thus it seems that the initial tendency is to move to the steady state with the lower minima, but this solution is unstable and will soon adjust to form the other steady state where it will remain. Similar behaviour was observed for larger β also, near the critical value for drawdown.

Tuck and Vanden Broeck [13], showed that at $F \approx 0.58, \beta = 0$ there is a unique, steady solution in which the free surface contains a cusp in the free surface above the sink. It has

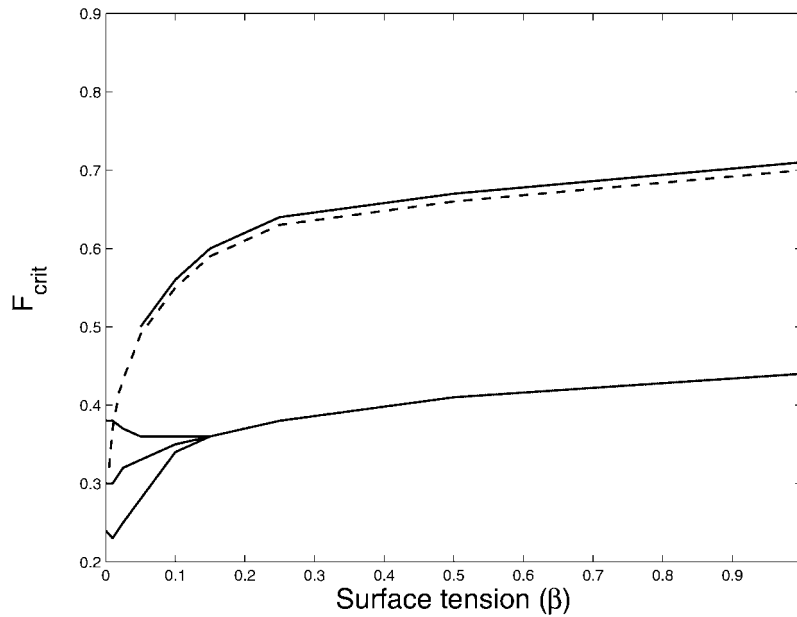


Figure 9. Critical F against β , image sink case, from simulations (solid top curve - minimal F to guarantee drawdown, dashed curve - maximum F for steady state) and single sink critical values (lower solid curve).

been conjectured that this cusp solution is a precursor to drawdown, and evidence for this was provided in [10]. However, for $\beta = 0.025$, the critical drawdown value seems to be around $F = 0.63$; for $\beta = 0.01$, this number drops to $F = 0.55$. If this trend continues, then with $\beta = 0$, an even lower value of F would be sufficient to induce a drawdown, throwing into doubt the importance of this unique solution.

Finally, we have conjectured that it is possible that the two-sink simulations represent an established flow after a long time. To support this, we performed a series of simulations with a single sink in which the sink intensity was slowly increased from around $F = 0.2$ up to a value of interest. Although the oscillations characteristic of the one sink case were still present, the long term behaviour paralleled quite closely the two-sink simulations. In all cases tried, the results were very similar: pinch-off occurred for similar values of F and movement to a steady state occurs in a similar way for lower F . These findings support the suggestion that the simulations with the image sink are equivalent to considering the long term behaviour of an established flow.

6. Conclusions

Numerical and asymptotic methods have been used to consider the unsteady flow generated by a line sink beneath a free surface. While there are a number of problems of academic interest, the most important consideration in terms of water quality modelling is whether the free surface is drawn down. It appears that the two situations considered in this paper are of great importance in determining this.

Considering the single sink case to be a model of the initiation of the flow from a fluid at rest, the critical value of F is determined by the size of the dip created above the sink as it is turned on. Once drawdown takes place, our numerical methods cannot determine what will

happen. It is possible that once such a flow is established, it will persist, but it is also possible that the free surface will bounce back up rather than remaining drawn down.

In the image-sink case (modelling a situation in which the strength of the sink is gradually increased to its final value) the drawdown behaviour is complicated by the formation of a central swell. Confusingly, the critical values overlap slightly the range of two-layer steady withdrawal flows (see [10]). It is possible that both solutions are possible and that which is chosen depends on the flow history.

It is worth re-stating the main findings regarding critical values. We do this for three typical values of β , starting with the largest value where things are clearest.

For $\beta = 0.15$, an impulsive start (no image sink) with F constant throughout, gives rise to steady states for $F \leq 0.35$, while a simple direct drawdown of the central point is observed for $F \geq 0.36$. However, for a non-impulsive start (image sink case), it appears that steady states can be maintained for $F \leq 0.59$, while if $F \geq 0.60$, a direct drawdown will occur. Similar behaviour occurs for $\beta > 0.15$.

For $\beta = 0.1$, things become a little less clear. An impulsive start gives rise to steady states for $F \leq 0.33$, while a direct drawdown is observed for $F \geq 0.36$. For the remaining values $0.34 \leq F \leq 0.35$, the simulation breaks down before it is clear whether a steady state or a drawdown will ensue (although some form of drawdown looks more likely). In the two sink case, it appears that steady states can be maintained for $F \leq 0.55$, given a suitable flow history, while if eventually $F \geq 0.56$, drawdown will result.

Finally, for $\beta = 0.05$, close to the smallest β for which clearly delineated results could be obtained, an impulsive start seems to lead to a steady state for $F \leq 0.24$, drawdown definitely appears to be averted for $0.25 \leq F \leq 0.27$, it is impossible to judge the long term behaviour for $0.28 \leq F \leq 0.30$, drawdown (albeit indirect) appears likely for $0.31 \leq F \leq 0.35$, while a direct drawdown appears certain for $F \geq 0.36$. In the image sink case, steady states appear to be achievable with a final value of F as high as 0.49, while above this value, drawdown seems certain, although it is probably indirect.

Reducing β blurs the picture still more, especially regarding drawdown, and for $\beta = 0$, not a great deal can be said. However, for $\beta = 0.02$, steady states have been observed to evolve and maintain themselves for final values of F of up to $F = 0.41$ (they are known to exist up to around 0.425); unfortunately drawdown critical values are not able to be pinned down. Steady states can be seen to evolve for β as small as 0.005.

Thus it appears that there are two possible critical values of Froude number at which drawdown may occur. The first opportunity for drawdown occurs during the initiation of the flow. If the starting Froude number is sufficient, then drawdown may be immediate. If not, then drawdown may not occur unless the flow rate is increased significantly (or the level of the free surface drops).

These results may go a long way to explaining the apparent discrepancies between all of the experimental results obtained in both the two dimensional and three dimensional withdrawals. The dependence of the upper value upon the initial shape of the free surface would add to this variability. Thus experiments starting with an initially deep lower layer may draw down at much higher values of F than those with shallower initial lower layers.

It would seem reasonable to speculate that flows with a very thin interface are unlikely to draw down with values of F much less than $F = 0.35$. However, the effect of the interface thickening is to decrease the effective gravity and make drawdown more likely at lower values of F . Thus flows with two layers separated by a thick interface could actually draw down at

very low values, see *e.g.* Jirka, [6], while with a thinner interface at somewhat higher values as in Hocking, [8].

As for the more academic questions, the unsteady results provide great insight into the withdrawal process. It certainly appears that there is a region of Froude numbers for which steady flows exist, possibly for any F below the critical drawdown value in the image-sink case, at least with $\beta \geq 0.05$. (If $\beta = 0$, steady flows are much harder to obtain using our methods.) Above a certain smaller critical value of F , an impulsive start seems to lead directly to drawdown. In spite of the difficulties of performing such numerical calculations, the numbers we have obtained, particularly in the presence of relatively little surface tension, agree well with steady results and taken together they give a clearer picture of the withdrawal process.

Appendix: small-time expansion details

In the small-time expansion

$$\phi(x, y, t) = \phi_0(x, y) + t\phi_1(x, y) + t^2\phi_2(x, y) + \dots, \quad (\text{A1})$$

expanding once more in y about $y = 0$ gives

$$\begin{aligned} \phi(x, y, t) = & \phi_0(x, 0) + t\phi_1(x, 0) + t^2\phi_2(x, 0) + t^3\phi_3(x, 0) + \dots \\ & + y\phi_{0y}(x, 0) + yt\phi_{1y}(x, 0) + yt^2\phi_{2y}(x, 0) + yt^3\phi_{3y}(x, 0) + \dots \\ & + \frac{1}{2}y^2\phi_{0yy}(x, 0) + \frac{1}{2}y^2t\phi_{1yy}(x, 0) + \frac{1}{2}y^2t^2\phi_{2yy}(x, 0) + \frac{1}{2}y^2t^3\phi_{3yy}(x, 0) + \dots \\ & + \frac{1}{6}y^3\phi_{0yyy}(x, 0) + \frac{1}{6}y^3t\phi_{1yyy}(x, 0) + \dots \end{aligned} \quad (\text{A2})$$

We substitute

$$\eta(x, t) = t\eta_1(x) + t^2\eta_2(x) + t^3\eta_3(x) + t^4\eta_4(x) + t^5\eta_5(x) + \dots \quad (\text{A3})$$

in this expression and the result in Equations (7) and (8) in such a way that all possible coefficients of powers of t up to degree three in (7) and four in (8) are accounted for. Thus we need all ϕ_t , ϕ_x and ϕ_y terms having combined t and y degrees of at most three, three and four respectively. Thus,

$$\begin{aligned} \phi_t = & \phi_1 + y\phi_{1y} + \frac{1}{2}y^2\phi_{1yy} + \frac{1}{6}y^3\phi_{1yyy} + 2t\phi_2 + 2ty\phi_{2y} + 2ty^2\phi_{2yy} \\ & + 3t^2\phi_3 + 3t^2y\phi_{3y} + 4t^3\phi_4 + \dots, \end{aligned} \quad (\text{A4})$$

$$\begin{aligned} \phi_x = & \phi_{0x} + t\phi_{1x} + t^2\phi_{2x} + t^3\phi_{3x} + y\phi_{0yx} + yt\phi_{1yx} + yt^2\phi_{2yx} + yt^3\phi_{3yx} \\ & + \frac{1}{2}y^2\phi_{0yyx} + \frac{1}{2}y^2t\phi_{1yyx} + \frac{1}{6}y^3\phi_{0yyyx} \end{aligned} \quad (\text{A5})$$

and

$$\begin{aligned}
\phi_y = & \phi_{0y} + t\phi_{1y} + t^2\phi_{2y} + t^3\phi_{3y} + t^4\phi_{4y} \\
& + y\phi_{0yy} + yt\phi_{1yy} + yt^2\phi_{2yy} + yt^3\phi_{3yy} + \frac{1}{2}y^2\phi_{0yyy} + \frac{1}{2}y^2t\phi_{1yyy} + \frac{1}{2}y^2t^2\phi_{2yyy} \\
& + \frac{1}{6}y^3\phi_{0yyyy} + \frac{1}{6}y^3t\phi_{1yyyy} + \frac{1}{24}y^4\phi_{0yyyyy},
\end{aligned} \tag{A6}$$

where all are evaluated on the line $y = 0$ at time $t = 0$.

Now substituting $\eta(x, t)$ to fifth order as above for y in each of these three equations and then substituting the result in Equation (7), collecting powers of t , and equating the constant term and coefficients of t , t^2 , and t^3 , respectively, to zero, all using the computer algebra package *Maple*, we obtain the dynamic conditions

$$\phi_1 + \frac{1}{2}(\phi_{0x}^2 + \phi_{0y}^2) = 0, \tag{A7}$$

$$\phi_{0x}\phi_{1x} + 2\phi_2 + \phi_{0x}\eta_1\phi_{0yx} + \eta_1\phi_{1y} + \phi_{0y}\eta_1\phi_{0yy} + \phi_{0y}\phi_{1y} + (\eta_1 - \beta\eta_{1xx}/F^2) = 0, \tag{A8}$$

and two others which we do not list here. Similarly, substituting in (8) and equating coefficients to zero gives five kinematic conditions, the first three of which are

$$\eta_1 - \phi_{0y} = 0, \tag{A9}$$

$$-\phi_{1y} - \eta_1\phi_{0yy} + \eta_{1x}\phi_{0x} + 2\eta_2 = 0, \tag{A10}$$

and

$$\eta_{1x}\eta_1\phi_{0yx} + \eta_{1x}\phi_{1x} - \eta_1\phi_{1yy} + \eta_{2x}\phi_{0x} + 3\eta_3 - \frac{1}{2}\eta_1^2\phi_{0yyy} - \eta_2\phi_{0yy} - \phi_{2y} = 0. \tag{A11}$$

Thus it is possible to determine ϕ_1 from the dynamic condition providing ϕ_0 is known, and η_1 from the kinematic condition; then ϕ_2 from the dynamic condition, and so on, until $\eta_1, \eta_2, \dots, \eta_5$ are found. The only non-trivial aspect of this is that in computing the ϕ_i , the dynamic conditions only give $\phi(x, 0)$, so in order to find $\phi(x, y)$ in general we must in effect solve Laplace's equation with a boundary condition, by extending $\phi_i(x, 0)$. This was automated on *Maple* also, as we now describe.

Given $f(x, 0) = g(x)$, to find $f(x, y)$ satisfying Laplace's equation means finding a complex potential function $w(z)$ for which (letting $z = x + iy$ with x, y real), $\Im(w(z)) = f(x, y)$; this means we must have $f(x, 0) = g(x)$. Of course, $w(z)$ will be unique given that it must be defined throughout the fluid, that is, for $y < 0$.

The potential function $w(z)$ may be determined using Poisson's integral formula, as in [19], but this can be rather laborious. Instead, experience suggests that it is possible to guess a general form for $w(z)$, and this has been implemented here. In practice, all $g(x)$ we encountered have the form $p(x)/(1 + x^2)^n$ where $p(x)$ is a polynomial with degree no more than $2n$. We assume $w(z) = q(z)/(z - i)^n$ (defined everywhere in the relevant half-plane and having a restriction to $z = x$ of roughly the right form), with $q(z)$ a polynomial in z of degree less than n . We then set $z = x + iy$ and use *Maple*'s complex number facility to determine the coefficients in $q(z)$ satisfying the condition $\Im(w(x)) = g(x)$. If this is successful, the resulting $w(z)$ must be the correct potential function and so $f(x, y) = \Im(w(x, y))$ is the relevant extension of $g(x)$ to cases where $y \neq 0$. In all cases considered this process was successful, and quite rapid.

References

1. J. Imberger and P.F. Hamblin, Dynamics of lakes, reservoirs and cooling ponds. *Ann. Rev. Fluid Mech.* 14 (1982) 153–187.
2. C.S. Yih, *Stratified Flows*. New York: Academic Press (1980) 418pp.
3. P. Gariel, Experimental research on the flow of nonhomogeneous fluids. *La Houille Blanche* 4 (1949) 56–65.
4. D.G. Huber, Irrotational motion of two fluid strata towards a line sink. *J. Engng. Mech. Div. Proc. ASCE* 86 (1960) 71–85.
5. I.R. Wood and K.K. Lai, Selective withdrawal from a two-layered fluid. *J. Hyd. Res.* 10 (1972) 475–496.
6. G.H. Jirka, Supercritical withdrawal from two-layered fluid systems, Part 1 Two-dimensional skimmer wall. *J. Hyd. Res.* 17 (1979) 43–51.
7. G.A. Lawrence and J. Imberger, Selective withdrawal through a point sink in a continuously stratified fluid with a pycnocline. *Tech. Report No. ED-79-002*, Dept. of Civil Eng., University of Western Australia, Australia (1979).
8. G.C. Hocking, Withdrawal from two-layer fluid through a line sink. *J. Hydr. Engng. ASCE* 117 (1991) 800–805.
9. G.C. Hocking and L.K. Forbes, Supercritical withdrawal from a two-layer fluid through a line sink if the lower layer is of finite depth. *J. Fluid Mech.* 428 (2001) 333–348.
10. G.C. Hocking, Supercritical withdrawal from a two-layer fluid through a line sink. *J. Fluid Mech.* 297 (1995) 37–47.
11. C. Sautreaux, Mouvement d'un liquide parfait soumis à lapesanteur. Détermination des lignes de courant. *J. Math. Pures Appl.* 7 (1901) 125–159.
12. A. Craya, Theoretical research on the flow of nonhomogeneous fluids. *La Houille Blanche* 4 (1949) 44–55.
13. E.O. Tuck and J.M. Vanden Broeck, A cusp-like free-surface flow due to a submerged source or sink. *J. Aust. Math Soc. Ser. B* 25 (1984) 443–450.
14. G.C. Hocking, Cusp-like free-surface flows due to a submerged source or sink in the presence of a flat or sloping bottom. *J. Aust. Math Soc. Ser. B* 26 (1985) 470–486.
15. J.M. Vanden Broeck and J.B. Keller, Free surface flow due to a sink. *J. Fluid Mech.* 175 (1987) 109–117.
16. D.H. Peregrine, A line source beneath a free surface. Rept. No. 1248, Math Res. Centre, University of Wisconsin, Madison (1972).
17. G.C. Hocking and L.K. Forbes, A note on the flow induced by a line sink beneath a free surface. *J. Aust. Math Soc. Ser. B* 32 (1991) 251–260.
18. L.K. Forbes and G.C. Hocking, On the computation of steady axi-symmetric withdrawal from a two-layer fluid. *Comp. Fluids* 32 (2003) 385–401.
19. P.A. Tyvand, Unsteady free-surface flow due to a line source. *Phys. Fluids A* 4 (1992) 671–676.
20. M. Xue and D.K.P. Yue, Nonlinear free-surface flow due to an impulsively started submerged point sink. *J. Fluid Mech.* 364 (1998) 325–347.
21. T. Miloh and P.A. Tyvand, Nonlinear transient free-surface flow and dip formation due to a point sink. *Phys. Fluids A* 5 (1993) 1368–1375.
22. L.K. Forbes and G.C. Hocking, Flow induced by a line sink in a quiescent fluid with surface-tension effects. *J. Austral. Math. Soc. Ser. B* 34 (1993) 377–391.
23. D. Scullen and E.O. Tuck, Non-linear free-surface flow computations for submerged cylinders. *J. Ship Res.* 39 (1995) 185–193.
24. E.O. Tuck, Solution of nonlinear free-surface problems by boundary and desingularised integral equation techniques. In: J.Noye (ed.), *Proc. 8th Binnial Computational Techniques and Applications Conference*, World Scientific (1997) pp. 11–26.
25. G.C. Hocking and L.K. Forbes, Flow induced by a line sink in a quiescent fluid with surface-tension effects. *J. Aust. Math Soc. Ser. B* 34 (1993) 377–391.